Kinematics of a manipulator with 1-DOF joints controlled by elastic, inner ties

Dominik Ozog[1*] , Ryszard Leniowski[1]

[1] Department of Computer and Control Engineering, Rzeszow University of Technology, al. Powstancow Warszawy 12, 35-959 Rzeszów, Poland
* Corresponding author's e-mail: d.ozog@prz.edu.pl

ABSTRACT

This paper presents a mathematical model of forward and inverse kinematics for a manipulator composed of joints with one degree of freedom allowing only the rotation of a Cartesian coordinate system around one axis. The manipulator is controlled by means of internal ties running from the point of connection with the controlled arm to the place of connection with the mechanism regulating the length of the individual tie. This length is the basis in derived equations, and its change is the direct cause of the movement of the described robot. In contrast to the commonly used arm drives, the articulated variable in derived kinematic equations is the length of the tie, which affects the change in the angle between the arms, while it is not the same value of this angle. In addition, these joints are arranged parallel to each other, which results in the working space of the manipulator in one plane. The kinematic chain, which is the object of the described research, consisted of three series connected joints enabling rotation around one axis of the coordinate system. However, the dependencies and formulas enabling their application to the description of forward kinematics and inverse kinematic chains built from a larger number of similarly arranged joints were demonstrated. The kinematics model presented in the paper proves that it is possible to independently control each of the serially connected joints using internal ties.

Keywords: 1-DOF joint, forward kinematics, inverse kinematics, ties, inner ties, manipulator.

INTRODUCTION

There are many publications relating to the issues of the kinematics model of manipulators made of joints with one degree of freedom, which is a rotation. Examples of these are [1, 2, 3]. However, the articulated variable in these articles is the rotation angle. The movement of arms depends on it. The joint through the gears is connected to the drive unit [4]. This construction makes it possible to trivially convert the rotation angle of the drive unit into a rotational movement of the arm. This concept has been known for many years and very often uses the Denavit-Hartenberg notation in calculations. A different situation occurs when using ties to control the manipulator. This solution is known from medical applications, in particular from the construction of a laparoscope [9] or more complex laparoscopic systems [10, 11].

Instead of gears converting the rotary motion of the driving motor into the angular rotation of the arm, these devices use internal cables to transfer the pulling forces – ties. In the case where one end of the tie is rigidly connected to the selected arm, the movement of this arm can affect changes in the length of the tie or changes in the point of engagement of the other end. The use of this type of mechanism is widely known, especially in the field of medicine, but the force acting on the tie is always the result of the operator's action on one of the ends of the tie. Often, a lever transmission is used to achieve greater precision. There is a publication [5] that discussed the model of direct and inverse kinematics and dynamics for a single joint controlled using internal ties. However, there is no known mathematical model for many such joints connected in series. This paper describes the kinematics model of a manipulator

consisting of any number of series-connected joints. The concept of such a robot is presented, for example, in the document [11]. It should be noted that the lack of presented kinematic models of such mechanisms in the literature may affect their low popularity. This article, by presenting a mathematical description, aimed to contribute to an increase in the number of applications for manipulators controlled by internal ties, not only through the direct effect of the operator's movements on the ties, but also by facilitating the use of electromechanical drives to affect the ties and creating systems that automatically control them.

The kinematics model presented in this paper uses the D-H notation, but introduces one small change. The classic D-H notation and the extended D-H notation describe the relationship between the manipulator's tool center point (TCP) and the rotation angles of individual joints. In the case of control using cables, the joint rotation angle is the result of changing the length or attachment points of the cables. Hence, the joint rotation angle is not a variable, but a function that takes the length of the tie as a variable. As a result, the presented kinematics model based on the D-H notation will describe the equations between the manipulator's TCP and the lengths of individual tiles. As a disadvantage of such a solution, one can mention the need to use more computing power to determine the trajectory of the robot's movement. However, the solution with internal ties makes it possible to achieve the degree of miniaturization of the manipulator that was not possible using the previously described drive mechanisms, which is discussed in paper [5].

The principle of control based on internal ties consists in changing the length of the tie while maintaining constant co-ordinates of its origin in the global reference system or changing its starting point or maintaining a constant length of the tie. A combination of both variants is also possible. In this case, the tie is controlled by changing the position of one end of it. This can be done by using a screw mechanism to which the tie is attached indirectly. Then, by turning the screw, the position of the system is forced to change, which forces the pull rod to be pulled. In the further course, the tie must run through the hole of the sleeve, which forces a constant position of the tie in this section. At the end of this sleeve, a point should be taken, which in further calculations will be considered the beginning of the position of the tie. In the remainder of this publication, this point has been marked with the letter A_i (Fig. 1), where

i is the number of the tie rod. From the starting point, the tie extends into the rotary joint sleeve. In this sleeve, there is a hole, both ends of which are inside the hinge on the side surface of the roll. One of these holes is located on the side of the i-th arm, while the other on the side of the $i+1$ arm manipulator. Through these points, a tie runs from the side of the previous arm and from the side of the other arm. The places from which the tie enters and exits the sleeve will be appropriately marked with the letters B_{ji} and C_{ji} (Fig. 1), where i – like previously – is the number of the tie rod, while j is the next number of the joint. In the second and in the following arms of the manipulator, the tie can be guided in two ways. The first is the end of the tie, through its rigid connection to the inner wall of the arm, and which will affect the tie. The second method is to guide the rod to the hole in the sleeve of the next joint and consequently to the next arm. Inside this arm, some of the ties are connected to it again and are responsible for its control. However, the other ties carried out in an analogous manner are responsible for subsequent parts of the manipulator. The points of the rigid connection of the end of the tie with the robot's arm will be denoted by D_i in the further part of the work (Fig. 1) while retaining the earlier meaning of the index.

For the control used so far in medical laparoscopes, which uses a single internal rod, there are no known kinematic models. This limits the possibility of developing medical procedure simulators using computer engineering tools, which are very important at the stage of educating medical staff and developing doctors' skills [20, 21]. Moreover, for cases such as those described in [22, 23] and [24] only direct control of the laparoscope by the surgeon is possible, which takes into account only the movement of the laparoscope tip, but does not allow for controlling its individual joints. Hence, this paper proves that it is possible to develop another control using 1-DOF joints and internal rods, which will allow for a mathematical description of the position of the joints of such a manipulator, and it will also be possible to control individual joints.

CONTROLLED OBJECT

Description of the kinematics of a single joint is presented in publication [5]. In contrast, the manipulator subjected to a mathematical description
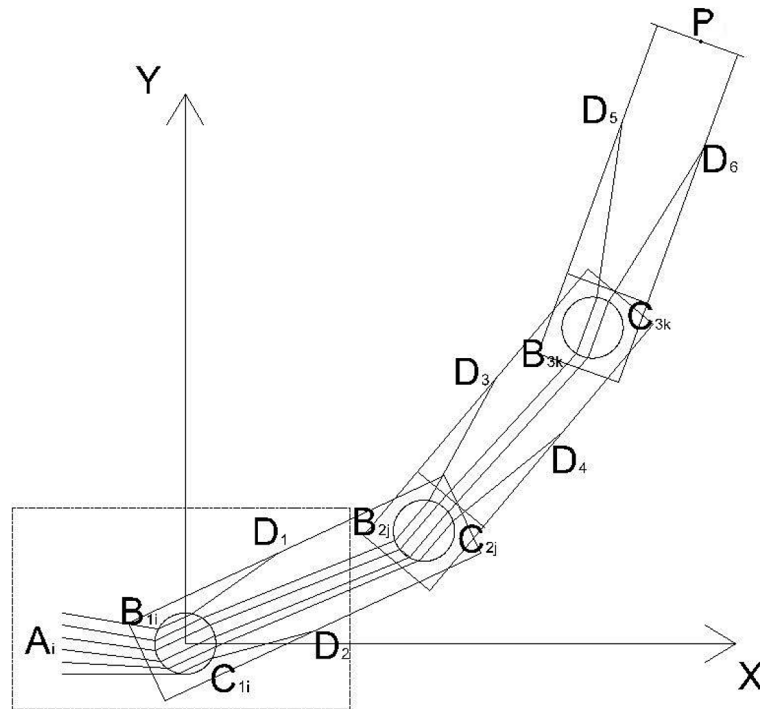
Figure 1. The scheme of a manipulator using internal ties

consists of three arms and six ties. Each arm is controlled by two ties. The ties are connected to the arm on opposite sides. This combination allows the pulling forces transmitted by these ties to act on the two sides of the arm. This allows forcing its torque in both directions. As it can be seen in Fig. 1, all starting points A_i are derived from the construction of the manipulator's arms. Such operation aims at moving the propulsion systems beyond the arms of the manipulator, which generate forces transmitted by the strands to the arms. Such operation allows performing a large miniaturization of the robot. This is done by the possibility of reducing the diameter of the arms,

inside which there must be no gears, drive units and wires supplying energy to these units. In the proposed solution, only the ties run through the arms. In the arms that are more and more distant from the base point, the number of these ties is smaller, which additionally allows for a further reduction in their diameter.

In Figure 1, the coordinates of the points have been represented in a symbolic manner using indices from 1 to 6 points. This simplification is intended to increase the readability of the drawing. In this case, the subsequent indices are in the following ranges: $i \in \langle 1,6 \rangle$, $j \in \langle 1,4 \rangle$, $k \in \langle 1,2 \rangle$, $i,j,k \in Z$. Figure 2 is an enlarged view of an area which in Fig.
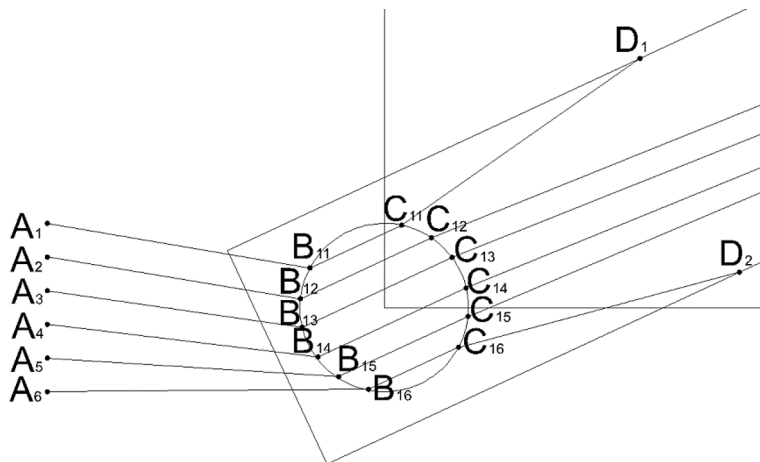

Figure 2. Enlarges a fragment of the scheme from Figure 1

1 has been covered by a dashed line. This diagram shows the waveforms of individual ties and the points between them run inside the sleeve.

Figure 2 shows a variant in which the points of entry and exit of the tie rod from the sleeve are parallel to each other and run at a constant distance expressed on the axis OY. This variant has been chosen to preserve the readability of the drawing. All formulas shown below will be met for any location of B_{ji} and C_{ji} points. It is also possible to place them in the XZ plane parallel to the OX axis at various distances expressed on the OZ axis. This variant is the easiest to obtain in the production process, because in both cases it is necessary for the pin connecting the arms to be immobilized relative to one of them. This immobilization can be achieved by locally changing the shape of the pin, using the previous pin or a cotter pin. In each of these situations, it requires additional fastening operations performed by the assembler or an appropriate mechanism that must reach this place. Reaching the inner arm is problematic due to limited access to the size of its internal hole. Hence, the variant with bearings used in the second, inner arm and the use of pin locks on the first, outer arm allows for greater freedom of movement for the assembler.

Two variants of joints

The manipulator presented in this paper is a simplified model of a manipulator consisting of three universal joints, i.e. joints with two degrees of freedom (two rotations), as described in [5]. If in each of these joints you prevent one of the two rotations and set them in a way that will cause the only possible rotation to take place around the OZ axis, then the effector's tip will move in the XY plane, which presents a simplified diagram shown in Figure 1. However, the universal joint consists of two different joints with one degree of freedom [5].
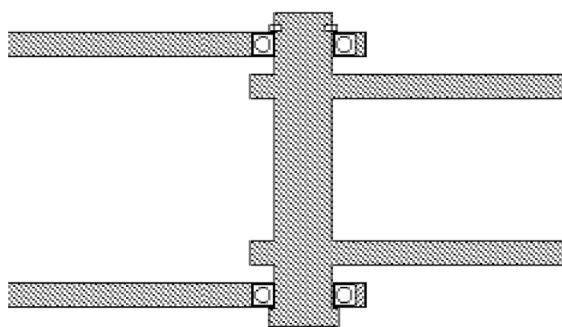
One of these joints concerns a situation in which the sleeve connecting the first and second manipulator arms is in rigid connection with the last arm, as shown in Figure 3. In contrast, when the bearing is applied, rotation relative to the first of the arms about an axis extending longitudinally through the center of the sleeve. The second part of the universal bushing in the universal joint is differently connected to the arms. This situation is shown in Figure 4. The sleeve is rigidly connected to the first arm. In contrast, contact with the other is bearing, which causes its rotation relative to the first and the sleeve. This difference affects the length of the tie passing through the manipulator built from one or the other type of joints [5].

KINEMATICS

In the further part of the article the coordinates of points A, B, C and D in the coordinate system will be marked by a small letter x, y or z together with the subscript, in which the point symbol will be saved. Despite considering the effector movement in two-dimensional space, all equations have been determined for three-dimensional space with the need to coordinate for each point. This is to enable the use of derived equations to be implemented after minor adjustments in the kinematics description of the manipulator composed of three universal joints connected in series.

Kinematics of the tie

Figure 5 shows the symbolic construction of the manipulator with the rotation symbols marked on it. The first arm rotates by angle α1 relative to the basic coordinate system. From the center of the pivot point of the first arm to the
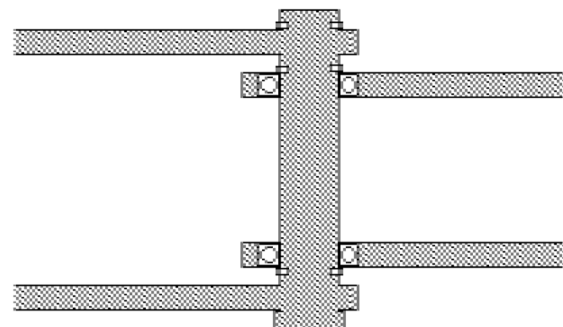

Figure 3. The first variant 1-DOF joint

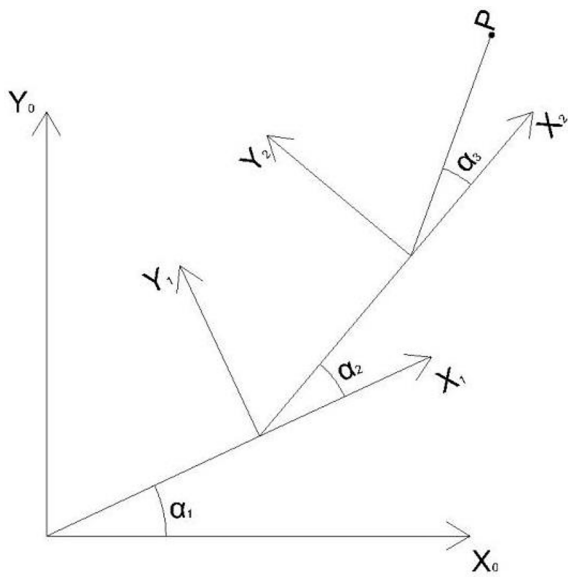**Figure 4.** The second variant 1-DOF joint

Figure 5. The second variant 1-DOF joint

pivot point of the second arm, the length of the first arm is determined as L1. The second arm rotates by angle $\alpha 2$ relative to the system displaced by the rotation angle and the length of the first arm and has a length L2 to the pivot point of the third arm. Similarly, the last arm rotates in the local system determined by the two aforementioned angles and lengths by $\alpha 3$. The length of the third arm is measured from the point of its rotation to its physical end, where the effector is marked by the point P.

Let $f(A, B)$ denote the function that takes two points and calculates the Euclidean distance between them [6].

$$f(A,B) = \sqrt{(x_B - x_A)^2 + (y_B - y_A)^2 + (z_B - z_A)^2} \quad (1)$$

After rotation by any angle α, the original points are displaced according to the equations given below:

$$B'_{ij} = \prod_{p=1}^{i}\left(R(\alpha_p, L_p)\right)B_{ij}$$

$$C'_{ij} = \prod_{p=1}^{i}\left(R(\alpha_p, L_p)\right)C_{ij} \quad (2)$$

$$D'_j = \prod_{p=1}^{\left[\frac{j}{2}\right]}\left(R(\alpha_p, L_p)\right)D_j$$

where: $i\in<1,3>$, $j\in<1,6>$, $i,j\in\mathbb{Z}$ and

$$R(\alpha_p, L_p) = \begin{bmatrix} \cos(\alpha_p) & -\sin(\alpha_p) & 0 & L_p\cos(\alpha_p) \\ \sin(\alpha_p) & \cos(\alpha_p) & 0 & L_p\sin(\alpha_p) \\ 0 & 0 & 1 & 0 \\ 0 & 0 & 0 & 1 \end{bmatrix} (3)$$

Equations 2 and 3 follow directly from the Denavit-Hartenberg convention [7].

If the length of the first or second tie is defined by li – according to the numbering shown in

Fig. 1 and Fig. 2 – then it can be expressed with the function f as (4).

$$l_i = f(A_i, B'_{1i}) + f(B'_{1i}, C'_{1i}) + f(C'_{1i}, D'_i), i \in \{1,2\}(4)$$

If the joint is used in the first variant (joint sleeve joined to the second arm), it should be noted that the two functions in (4) always have the same value [5] regardless of the angle of rotation $\alpha 1$. What can be saved as (5).

$$\begin{aligned} f(B'_{1j}, C'_{1j}) &= f(B_{1j}, C_{1j}) \\ f(C'_{1i}, D'_i) &= f(C_{1i}, D_i) \end{aligned} \quad (5)$$

where: $i\in<1,2>, j\in<1,6>, i,j\in\mathbb{Z}$.

From (5) it follows that the length of sections between points B1i, C1i and C1i, Di for $i\in\{1,2\}$ is constant. Similar equations can be derived for subsequent wrists. In the considered case, these are joints 2 and 3; however, the equations can be extended for any number of manipulator arms (6).

$$\begin{aligned} f(B'_{ij}, C'_{ij}) &= f(B_{ij}, C_{ij}) \\ f(C'_{ii}, D'_i) &= f(C_{ii}, D_i) \quad (6) \\ f(C'_{i(i+1)}, D'_{i(i+1)}) &= f(C_{i(i+1)}, D_{(i+1)}) \end{aligned}$$

where: $i,j\in\mathbb{N}+$ and i is the number of the joint, j is the number of the tie.

Using (6) it is possible for each tie to determine the characteristic value of l_p, which does not change. These values are presented in (7).

$$\begin{aligned} l_{pi} &= f(B_{1i}, C_{1i}) + f(C_{1i}, D_i) \\ l_{pj} &= f(B_{1j}, C_{1j}) + f(B_{2j}, C_{2j}) + f(C_{2i}, D_i) \\ l_{pk} &= f(B_{1k}, C_{1k}) + f(B_{2k}, C_{2k}) + \\ &\quad + f(B_{3k}, C_{3k}) + f(C_{3k}, D_k) \end{aligned} \quad (7)$$

where: $i\in\{1,2\}, j\in\{3,4\}, k\in\{5,6\}$.

The equation (7) can be written in a general form (8) for any number of articulations, while keeping the numbering as in Fig. 1 and Fig. 2.

$$l_{pi} = f\left(C_{\left[\frac{i}{2}\right]i}, D_i\right) + \sum_{j=1}^{\left[\frac{i}{2}\right]} f(B_{ji}, C_{ji}), i \in \mathbb{N}_+ (8)$$

From (4) and (8) a simplified equation (9) can be obtained.

$$l_i = f(A_i, B'_{1i}) + l_{pi}, i \in \{1,2\} \quad (9)$$

From (9) one can calculate the angle value $\alpha 1$, which is presented in [5]. This is possible because as a result of the function $f(A_i, B'_{1i})$, $i\in\mathbb{N}+$ is associated only with the angle $\alpha 1$. This is a very important relationship that can be used to calculate the values of other angles. By using (1), (2) and

(7) the lengths of ties numbered 3 and 4 can be represented as (10).

$$l_i = f(A_i, B'_{1i}) + f(C'_{1i}, B'_{2i}) + l_{pi}, i \in \{3,4\} \quad (10)$$

In (10) the only unknown values contain the expression $f(C_{1i}', B_{2i}')(C_{1i}', B_{2i}')$. The value of l_{pi} is constant, while $f(A_i, B_{1i}')$ can be calculated from (9) using the transformations described in [5]. By transforming (10) one obtains (11).

$$a_i \cos(\alpha_2) + b_i \sin(\alpha_2) = c_i$$
$$, where$$
$$a_i = 2L_1 x_{B_{2i}} - 2x_{B_{2i}} x_{C_{1i}} - 2y_{B_{2i}} y_{C_{1i}}$$
$$b_i = 2x_{C_{1i}} y_{B_{2i}} - 2x_{B_{2i}} y_{C_{1i}} - 2L_1 y_{B_{2i}}$$
$$c_i = \left(l_i - l_{pi} - f(A_i, B'_{1i})\right)^2 - \left(L_1 - x_{C_{1i}}\right)^2 - \quad (11)$$
$$-\left(z_{B_{2i}} - z_{C_{1i}}\right)^2 - x_{B_{2i}}^2 - y_{B_{2i}}^2 - y_{C_{1i}}^2$$
$$i \in \{3,4\}$$

It is also possible to deduce on the base (11) the generalized patterns for the k joint, where $k \geq 3$ (12).

$$a_i \cos(\alpha_k) + b_i \sin(\alpha_k) = c_i$$
$$, where$$
$$a_i = 2L_m x_{B_{ki}} - 2x_{B_{ki}} x_{C_{mi}} - 2y_{B_{ki}} y_{C_{mi}}$$
$$b_i = 2x_{C_{mi}} y_{B_{ki}} - 2x_{B_{ki}} y_{C_{mi}} - 2L_m y_{B_{ki}}$$
$$c_i = \left(l_i - l_{pi} - f(A_i, B'_{1i}) - \sum_{n=2}^{m} f(C'_{ni}, B'_{(n+1)i})\right)^2 - \quad (12)$$
$$-\left(L_m - x_{C_{mi}}\right)^2 - \left(z_{B_{ki}} - z_{C_{mi}}\right)^2 - x_{B_{ki}}^2 -$$
$$-y_{B_{ki}}^2 - y_{C_{mi}}^2$$
$$k \geq 3$$
$$m = k - 1$$
$$i \in \{2k - 1, 2k\}$$

From (11) or (12) and trigonometric identities [8], equations analogous to those in [5] are obtained. The mentioned dependences are obtained (13).

$$\alpha_k = \{\alpha_k \in \mathbb{R} : \alpha_k \in \alpha_{2k-1} \wedge \alpha_k \in \alpha_{2k}\}, where$$
$$\alpha_i = \tan^{-1}\left(\frac{b_i}{a_i}\right) + \tan^{-1}\left(\frac{\pm\sqrt{a_i^2 + b_i^2 - c_i^2}}{c_i}\right) \quad (13)$$

It should be noted that the calculation of angle values is a recursive task and it is possible to determine them for k only if their values for k-1 are known, where $k \in N+$. In addition, variables a, b and c from (11) or (12) are used in (13).

Kinematics of the angle

The derivation above showed how to calculate the position angles of the arms knowing the length of the ties. The values of these angles can be used when calculating the position of the effector P. The coordinates of this point and its orientation can be read from the DH notation after the calculation (14).

$$P' = \prod_{p=1}^{3} R(\alpha_p, L_p) \quad (14)$$

In the case of the described manipulator, inverse kinematics requires two stages of calculation. The first is to determine the angles of the rotation of the arms, and then knowing them one can calculate the lengths of the ties. When the coordinates of the P' point are known, it must be determined whether it is in the manipulator's workspace. For this purpose $R1(L1\cos(\alpha1), L1\sin(\alpha1), 0)$, will be entered. This point describes the coordinates of the tip of the first arm. In the initial simplification, it was assumed that all points in the radius $L2 + L3$ from the point $R1$ are within the scope of the manipulator.

Starting from the wheel Equation 15, they can be transformed to find the range of the $\alpha1$ angle for which the point P' will be in range (16).

$$\left(x_{P'} - x_{R_1}\right)^2 + \left(y_{P'} - y_{R_1}\right)^2 - (L_2 + L_3)^2 \leq 0 \quad (15)$$

$$x_{P'} \cos(\alpha_1) + y_{P'} \sin(\alpha_1) \geq \frac{(L_2 + L_3)^2 - x_{P'}^2 - y_{P'}^2 - L_1^2}{-2L_1} \quad (16)$$

As mentioned earlier, the range given in (16) concerns the unlimited rotational possibilities of the first joint. In order to include in the considerations the physical construction of the manipulator, its permissible range was introduced for each joint (17).

$$\alpha_i \in \langle \beta_{MINi}, \beta_{MAXi} \rangle, i \in \mathbb{N}_+ \quad (17)$$

From (16) and (17) were obtained (18).

$$\alpha_1 \in \langle -\gamma_1, \gamma_1 \rangle \cap \langle \beta_{MIN1}, \beta_{MAX1} \rangle, where$$
$$\gamma_1 = \tan^{-1}\left(\frac{y_{P'}}{x_{P'}}\right) + \tan^{-1}\left(\frac{\sqrt{x_{P'}^2 + y_{P'}^2 - d_1^2}}{d_1}\right) \quad (18)$$
$$d_1 = \frac{(L_2 + L_3)^2 - x_{P'}^2 - y_{P'}^2 - L_1^2}{-2L_1}$$

Because the manipulator under study is a redundant system, the results of inverse kinematics calculations are ranges and sets of values. Equation 18 derives the range that can be taken by the $\alpha1$ angle. The calculation of the remaining angle values will be based on the $\alpha1$ values selected from the range (18). This form of calculating inverse kinematics for a redundant manipulator allows for the implementation of a trajectory whose aim is to minimize the displacement of the first joint. This form of traffic is used due to lower energy consumption and greater traffic dynamics. This is due to larger movements usually with lighter arms that

are closer to the effector instead of the heaviest and often the largest arms close to the base point. Such movement is also natural for many operations performed by man. In a situation where the range of motion is within wrist range, people rarely use the arm joint, although a desirable hand position can be achieved by using each of these joints. However, if there is a need to minimize the movement in the last wrist, you can easily reverse the presented algorithm by calculating instead of R1the point R2, which is the beginning of the third arm and assuming that its end is at P 'and then checking whether within the range of the remaining arms is the point with coordinates (0, 0, 0).

Equation 18 allowed checking whether the point is not too far from the assumed origin of the coordinate system to be in the workspace. Knowing (17) the limits for other joints, you can check whether the point is too close to the origin of the coordinate system. For this purpose, analogous wheel equations should be derived for all combinations of the minimum and maximum values of the remaining joints, and then checked whether the coordinates of the point are greater than any of the designated circles. However, it is proposed to apply me to complex calculations. For this purpose, the distance r_m between the points P' and R1 should be calculated (19).

$$r_m = \sqrt{\left(x_{P\prime} - x_{R_1}\right)^2 + \left(y_{P\prime} - y_{R_1}\right)^2} \quad (19)$$

After determining the length of the segment r_m, one should check what values can take the α_3 angle in the triangle $L_2\, L_3\, r_m$, in which the α_3 angle is opposite the segment r_m. To this end, the Heron's formula is applied to the area of the triangle (20).

$$S = \sqrt{p(p - L_2)(p - L_3)(p - r_m)}, where$$
$$p = \frac{1}{2}(L_2 + L_3 + r_m) \quad (20)$$

Using (20) and the formula on the area of the triangle using the length of two sides and the value of the angle between them two possible values of the angle α3 can be determined (21).

$$\alpha_3 \in \{-\alpha_{3part}, \alpha_{3part}\}$$

$$\alpha_{3part} = \tan^{-1}\left(\frac{2S}{L_2 L_3 \sqrt{1 - \left(\frac{2S}{L_2 L_3}\right)^2}}\right) \quad (21)$$

The above-mentioned formula cannot be directly used to calculate the value of the α2 angle

in the local coordinate system X1Y1 shown in Figure 5. It is proposed to appropriately convert the kinematics Equations 14 from which (22) is obtained.

$$\alpha_2 \in \{\alpha_{3\_1}, \alpha_{3\_2}\}$$

$$\alpha_{3\_i} = \tan^{-1}\left(\frac{b_i}{a_i}\right) + \tan^{-1}\left(\frac{\sqrt{a_i^2 + b_i^2 - c_i^2}}{c_i}\right)$$

$$,where \quad (22)$$
$$a_1 = L_2 \cos(\alpha_1) + L_3 \cos(\alpha_1 + \alpha_3)$$
$$b_1 = -L_2 \sin(\alpha_1) - L_3 \sin(\alpha_1 + \alpha_3)$$
$$c_1 = x_{P\prime} - L_1 \cos(\alpha_1)$$
$$a_2 = L_2 \sin(\alpha_1) + L_3 \sin(\alpha_1 + \alpha_3)$$
$$b_2 = L_2 \cos(\alpha_1) + L_3 \cos(\alpha_1 + \alpha_3)$$
$$c_2 = y_{P\prime} - L_1 \sin(\alpha_1)$$

The α_2 values based on (22) should be calculated for the previously adopted α_1 value and all possible α_3 values. Then, one should check if they are in the compartments (17).

RESULTS

The derived equations were verified on a real object. For this purpose, a station was built to control a single joint. Both the arms and the joint were printed on a 3D printer using FFF (Fused Filament Fabrication) printing technology. The outer diameter of the arms of the tested model was 20 cm, while the inner diameter was 18 cm. This directly influenced the position of the D_i points, which had coordinates D_1 (0 cm, 9 cm, 10 cm) and D_2 (0 cm, -9 cm, 10 cm). The calculations were based on the centimeter unit on the axes of the coordinate system and the coordinate system positioned in such a way that the z axis ran centrally along the axis of the first arm, while the joint rotated around the x axis. Similarly, points C_i have coordinates C_1 (0 cm, 4 cm, 1 cm) and C_2 (0 cm, -4 cm, 1 cm), while points B_i: B_1 (0 cm, 4 cm, -1 cm) and B_2 (0 cm, -4 cm, -1 cm). For the measurement station with one joint prepared in this way, tests were carried out to determine the dependencies of the actual length of the tie and the angle of rotation of the joint, and to compare them with the data resulting from the derived formulas.

Figure 6 shows a graph of changes in the length of the tie depending on the angle of rotation of the joint controlled using this tie. The values read on the physical station enabling control of the joint are marked in red, while the values
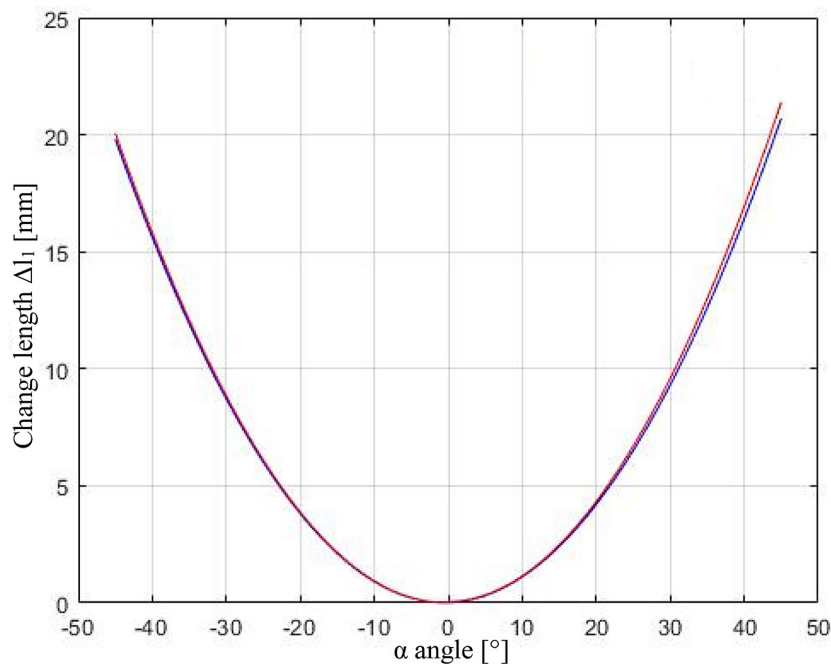
Figure 6. Dependencies of the change length of the tie and the angle of rotation of the joint

resulting from the kinematics model presented in this paper are marked in red. For negative values of the angle, i.e. rotation in the opposite direction than the point of attachment of the tie to the arm, it can be observed that the calculated and actual values match almost identically. The situation is different in the case of rotation towards the point of attachment of the tie to the arm wall – positive values. Up to a value of about 25° one can also speak of ideal representation of kinematics and actual readings; however, with the increase of the tie length, a model mismatch error appeared. From the angle value of 40° we can speak of a sudden increase in the error. It should be noted here that the tie used for the tests was a copper cable, with a copper purity degree of 4N, i.e. consisting of at least 99.99% copper. Young's modulus (which is responsible for longitudinal elasticity for elements made of a given material) for copper is about 120 GPa. At the same time, with the increase of the angle of rotation towards the tie attachment, the force that the arm exerts on the tie increases, increasing its tension. The increase in this force is not uniformly proportional to the value of the angle, but this relationship can be approximated as the square of the sine function. Hence, the increase in the discrepancy between the calculated and actual values shown in the graph results from the extensibility of the material from which the tie was made. The kinematic models currently

presented in the paper do not take into account the properties of the tie's material. In further work, the authors plan to extend these models and conduct tests for other materials with a higher Young's modulus, such as tungsten and titanium oxide.

DISCUSSION

This paper presents a metameric description of direct and inverse kinematics for a manipulator controlled by internal ties. In this model, the joint variables are not the angles of rotation of individual joints but the lengths of the ties acting on the subsequent arms of the manipulator. This work provides a theoretical basis for further research enabling the implementation of the presented mathematical model and enables the automation of precise control of manipulators using inner ties. The aim of the work is not only to describe the basic phenomena occurring in the discussed structure, but also to facilitate the application and increase the popularity of using such mechanisms.

Due to the lack of a large number of publications addressing exactly the same problem, it is not possible to make a collective comparison for exactly the same case. However, paper [5] also refers to joints controlled by inner ties, but the problem described therein concerns only a single

1DOF joint, which significantly limits the application of such a mechanism in real cases.

It is also important to note that the use of cables for robot movement is not new in industrial applications. Such concepts are presented in the review article [12]. It mainly concerns the construction of cable-driven parallel robots (CDPR). Most of the mechanisms described therein concern solutions in which cables are located on the outside of the manipulator structure, not inside. The last of the discussed models is an exception: low motion-noise humanoid head/neck simulator driven by seven cables, which can generate 1-DOF jaw movement and 3-DOF neck movement [12]. However, in this case, a spring was used to generate forces acting in the opposite direction to the forces transmitted by the ties [13].

The application of other designs using external cables is also widely presented in the review [14]. These solutions mainly focus on different CDPR models, for which the kinematics and dynamics model is widely known in the literature. The application for such robots is also widely known in industry, e.g. for automated warehousing, specifically for Automated Storage and Retrieval Systems [15] or in material processing [16]. Such solutions have basic control concepts widely discussed in the literature [17] and various variants of their improvement have been proposed [18]. However, for mechanisms with internal cables, the available literature is very poor. Hence, there is a need to describe the basic phenomena, which is part of this publication.

For the full picture of the situation, it is necessary to mention flexible manipulators, in which one of the concepts assumes the use of internal ties [19]. For them, the issues related to kinematics have been presented in the literature. However, due to the completely different characteristics of the joints, their kinematics do not relate to the solutions based on cylindrical joints discussed in this paper.

As part of further work on the subject of joint control using internal tendons, the authors plan to address the issues related to the vibrations generated during such control and the possibilities of their damping [25], the influence of different tendon materials on the precision of control [26] taking into account their extensibility, and the planning of complex trajectories [27] including the type of force transfer.

CONCLUSIONS

In this publication, the equations of forward and inverse kinematics for the manipulator manipulated using internal ties and constructed from three interconnected joints with one degree of freedom - rotation were derived, assuming that these joints work around one axis. The equations that allow calculating the coordinates of the effector tip are shown when the lengths of ties are known – the formulas (18), (21), (22) and (4) are used successively, or in the reverse situation, when the lengths of ties are known, the position of the end of the manipulator is it is possible to determine by using formulas (11), (13) and (14). In addition, the formulas (8), (12), (13) have been determined, which concern the problem of control by means of tie rods consisting of more arms than 3.*

REFERENCES

1. Zhang X., Zhang X., Chen Z Dynamic analysis of a 3-RRR parallel mechanism with multiple clearance joints. Mechanism and Machine Theory 2014; 78: 105–115.

2. Santos V., Valero-Cuevas F. Reported anatomical variability naturally leads to multi-modal distributions of Denavit-Hartenberg parameters for the human thumb. IEEE Transactions on Biomedical Engineering 2006; 53: 155–163.

3. Yoshikawa T. Manipulability of Robotic Mechanisms. The International Journal of Robotics Research 2016; 4: 3–9.

4. Kong K., Bae J., Tomizuka M. Control of rotary series elastic actuator for ideal force-mode actuation in human–robot interaction applications. IEEE/ASME Transactions on Mechatronics 2009; 14: 105–118.

5. Ożóg D. The modelling of two DOF joints controlled by elastic inner ties. In: Proc. of ITM Web Conf., Lublin, Poland 2017.

6. Maurer C., Rensheng Q., Raghavan V. A linear time algorithm for computing exact Euclidean distance transforms of binary images in arbitrary dimensions. IEEE Transactions on Pattern Analysis and Machine Intelligence 2003; 25: 265–270.

7. Leniowski R., Podstawy Robotyki. Uniwersytet Rzeszowski, 2005.

8. Rade L., Westergren B., Mathematics Handbook for Science and Engineering. Springer, 2004.

9. Debes A.J., Aggarwal R., Balasundaram I., Jacobsen M.B.J. Construction of an evidence-based, graduated training curriculum for D-box, a webcam-based laparoscopic basic skills trainer box. The American

Journal of Surgery 2012; 203(6): 768–775.

10. Heiliger T. Usability and performance studies of an augmented reality laparoscopic system for minimal invasive surgery. Dissertation zum Erwerb des Doktorgrades der Humanbiologie an der Medizinischen Fakultät der Ludwig-Maximilians-Universität zu München, 2023.

11. Brecht S.V., Voegerl J.S.A., Lueth T.C. Automated design and construction of a single incision laparoscopic system adapted to the required workspace. In: Proc. of 2020 IEEE/RSJ International Conference on Intelligent Robots and Systems (IROS), Las Vegas, NV, USA, 2020.

12. Qian S., Zi B., Shang WW. et al. A Review on cable-driven parallel robots. Chinese Journal of Mechanical Engineering 2018; 31(66).

13. Gao B., Xu J., Zhao J. et al. A humanoid neck system featuring low motion-noise. J Intell Robot Syst 2012; 67: 101–116.

14. Tang X. An Overview of the development for cable-driven parallel manipulator. Advances in Mechanical Engineering 2014; 6.

15. Khajepour A., Mendez S.T., Rushton M., et al. A warehousing robot: From concept to reality. Cable-Driven Parallel Robots. Mechanisms and Machine Science 2023; 132: 397–406.

16. Reichenbach T., Clar J., Pott A., Verl A. Adaptive preload control of cable-driven parallel robots for handling task. arXiv 2024; 2403.19293.

17. Guagliumi L., Berti A., Monti E., Fabritius M., Martin C., Carricato M. Force-sensor-free implementation of a hybrid position–force control for over-constrained cable-driven parallel robots. Robotics 2024; 13(2): 25.

18. Fabritius M., Rubio G., Martin C., et al. A nullspace-based force correction method to improve the dynamic performance of cable-driven parallel robots. Mechanism and Machine Theory 2023; 181(105177).

19. Wang H., Wang C., Chen W., Liang X., Liu Y. Three-Dimensional Dynamics for Cable-Driven Soft Manipulator. IEEE/ASME Transactions on Mechatronics 2017; 22(1): 18–28.

20. Danny S., Benjamin H. K., Alvin L., et al. Cost-effectiveness of virtual reality and wet laboratory cataract surgery simulation. Medicine 2023; 102(40):e35067.

21. Chahal B., Aydın A., Amin M.S.A., et al. Transfer of open and laparoscopic skills to robotic surgery: a systematic review. Journal of Robotic Surgery 2023; 17: 1207–1225.

22. Fukunaga T., Kasanami T. Single-incision laparoscopic repair for an arcuate line hernia: a case report. Surgical Case Reports 2021; 7: 196.

23. Zhao Q., Han H., Lei H., Li Y., Tian L., Xing N. A new surgical technique of laparoscopic retrograde inguinal lymph node dissection. Clinics of Surgery 2021; 6(4).

24. Dongen J.C. van, Versteijne E., Bonsing B.A., et al. The yield of staging laparoscopy for resectable and borderline resectable pancreatic cancer in the PREOPANC randomized controlled trial. European Journal of Surgical Oncology 2023; 49(4): 811–817.

25. Priyandoko G, Hunaini F, Imaduddin F, Ubaidillah U, Suwandono P, Sasongko M. I. N. Development of a vibration isolator on the basis of a magneto-rheological elastomer. Advances in Science and Technology Research Journal. 2024.

26. Karolewska K, Szala G, Trepczyńska-Łent M, Ligaj B. Improving the mechanical properties of structural elements made of titanium, aluminum alloys, and steel through the AM application. Advances in Science and Technology Research Journal. 2024.

27. Babiarz A, Kustra M, Wen S. Application of deep learning methods for trajectory planning based on image information. Advances in Science and Technology Research Journal. 2024; 18(6): 247–258. doi:10.12913/22998624/191924.